

Near-threshold excitation in light rare-earth compounds: A new interpretation of 3d appearance-potential spectra

H. Hinkers,* R. Stiller, and H. Merz

*Physikalisches Institut der Universität Münster, Wilhelm-Klemm-Strasse 10,
D-4400 Münster, Federal Republic of Germany*

(Received 27 March 1989)

A two-step model describing the transitions in electron-excited appearance-potential spectroscopy (APS) is presented for the 3d thresholds of La and Ce compounds. The model permits a consistent interpretation of APS spectra taken with different modes [soft x-ray APS (SXAPS), Auger-electron APS, disappearance-potential spectroscopy]. Within this model an investigation has been performed on La and Ce compounds exhibiting different valencies: LaB₆, CeB₆, and CeO₂. The spectra are discussed in terms of atomiclike 4f states. The fine structure reflects the multiplet structure of the excited configurations modified by state-selective excitation probabilities near the threshold and—in SXAPS—by dipole selection rules. The interpretation of the APS data is supported by comparison with multiplet calculations and core-level electron-energy-loss spectra recorded at low excitation energy.

I. INTRODUCTION

In the last two decades appearance-potential spectroscopy (APS) has developed into a sensitive method for the investigation of electronic properties of solid surfaces.¹⁻³ The method is based on the core-level excitation of atoms in a solid by electrons of well-defined energy. The excitation is monitored as a function of incident-electron energy via the decrease of elastically scattered electrons [disappearance-potential spectroscopy: DAPS (Ref. 4)] or by the detection of the various emission products, i.e., photons in the case of soft x-ray appearance-potential spectroscopy (SXAPS) (Refs. 1 and 2) and electrons in the case of Auger-electron appearance-potential spectroscopy (AEAPS).⁵⁻⁷ From APS measurements information can be obtained about core-level binding energies⁸⁻¹¹ as well as properties of the unfilled electronic states near the Fermi energy E_F .¹²

The APS transition process near the excitation threshold is rather complicated since the excitation leads to an electronic configuration which differs from the ground state by the presence of a core hole and two additional electrons near E_F , i.e., (i) the incident primary electron and (ii) the excited core electron. The corresponding spectral shapes are given by a two-particle density of states which in the case of 3d transition metals could successfully be described as the self-convolution of the one-particle density of states with correlation effects being generally neglected.¹²⁻¹⁴ This simple model cannot be transferred to rare earths (RE) and rare-earth compounds since the electronic structure near E_F is dominated by quasilocalized and highly correlated 4f states and the two-particle density of states should be completely different from the self-convolution of the one-particle density of states. Thus the determination of ground-state properties from APS data seems to be at first glance rather complicated as compared with similar spectroscopies such as x-ray absorption spectroscopy (XAS). What

makes APS, nevertheless, attractive as a spectroscopic method is its simplicity concerning the experimental set-up (no need of an energy analyzer); this is discussed in detail below. Furthermore, when applied to 4f systems APS offers the possibility of studying correlation effects very directly just because of the fact that two additional electrons are allowed to occupy the 4f level.

It is the scope of this work to give a new interpretation of the fine structure of APS spectra of light-RE systems. We explicitly use a two-step description of the APS process—the excitation step followed by the decay step. We have confined our work to compounds of the light RE's La and Ce. Among the light-RE elements, La is expected to be the simplest case for analysis since the ground state of the La³⁺ ion in a solid compound is described by the noble-gas configuration of Xe with empty 4f levels leading to rather simple multiplet structures of the excited configurations and the La 5d and 6s valence electrons are forming the conduction band. So, La compounds are expected to offer a good test of the APS model presented in this work. Ce offers the advantage of covering a range of different f counts or valencies: In most solid compounds Ce is trivalent with typically 0.7–1.0 4f electron in the ground state¹⁵⁻¹⁷ but in CeO₂ it is tetravalent with a 4f⁰ ground-state configuration.^{18,19} Thus the comparison of the corresponding spectra is expected to yield detailed information about the influence of the 4f occupation number on the fine structure of the APS spectra. Furthermore, La and Ce compounds have been subject to much theoretical and experimental work concerning their electronic structure so that a lot of additional data are available. Nevertheless, it was necessary for a quantitative explanation of the APS process to combine the APS results with our own core-level electron-energy-loss spectroscopy (CEELS) measurements. This combination of data together with multiplet data makes it possible to analyze the underlying electronic transitions in great detail allowing the in-

clusion of multiplet effects in the model. The basic ideas of the two-step model are presented in the following section.

II. THE MODEL

In DAPS the core-level excitation is monitored directly via the decrease of the current of the quasielastically reflected electrons.⁴ In SXAPS and AEAPS the excitation is monitored indirectly via the detection of the corresponding emission products which are created in the subsequent decay processes. Although the different APS spectra agree in gross structures they generally show different fine structures.⁷ The different APS versions should therefore not be considered as redundant but as complementary methods. In particular the combination of the different data yields detailed information about the APS process itself.

We have used a two-step model for the APS process involving the excitation step and the decay step. The two-step model allows a consistent description of the different APS versions. In terms of this model DAPS gives information directly about the excitation step whereas SXAPS and AEAPS spectra include additional information about the different channels in the decay step. This will turn out to be an important aspect concerning the explanation of the APS fine structure.

Figure 1 schematically shows the APS process with two different channels of the excitation step [1(a), 1(b)] and the decay steps for SXAPS [1(c), 1(d)] and AEAPS [1(e), 1(f)]. In the following we will consider only those transitions with at least one electron being excited to the $4f$ level. The two excitation channels which are assumed then to contribute to the APS intensity are shown in Figs. 1(a) and 1(b). The first one describes a transition with both the incident and the excited core electron occupying the $4f$ level and the second one describes a transition with one electron occupying the $4f$ level and the other electron being excited to an itinerant-electron state. One of the most important questions to be discussed in this paper concerns the relative contributions of these two excitation channels to the APS signal.

The dominant decay steps for SXAPS and AEAPS are shown in Figs. 1(c)–1(f). There are various decay channels leading to the emission of photons and electrons. For the interpretation of APS data it seems to be worthwhile to distinguish between two different types of decay channels. The first one describes ordinary characteristic x-ray emission and Auger emission processes with the $4f$ electrons as spectators. These processes are shown in Figs. 1(c) and 1(e). The second one describes emission processes with the excited $4f$ electrons being actively involved in the transitions. These processes are called x-ray recombination process²⁰ in the case of photon emission and direct recombination process²¹ in the case of electron emission and are shown in Figs. 1(d) and 1(f). The different decay channels as well as the excitation channels will be discussed in more detail below.

Within this paper the interpretation of the APS data will be performed in terms of atomiclike $4f$ states. Hybridization due to the coupling of $4f$ states with extended

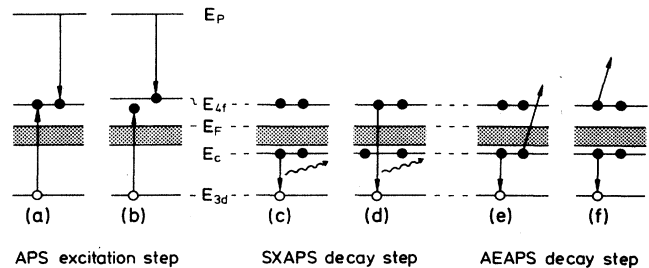


FIG. 1. Energy-level diagram for the APS two-step model describing the different excitation channels [(a), (b)] and decay channels for SXAPS [(c), (d)] and AEAPS [(e), (f)] schematically. In the excitation step a $3d$ electron is excited near the Fermi energy E_F by an incident electron with energy E_P . Only transitions with at least one electron being excited to the $4f$ level are considered here. Due to correlation effects the energy E_{4f} of the $4f$ level depends on the number of $4f$ electrons. For the decay step a distinction is made between two basically different decay channels: one describing characteristic x-ray emission in the case of SXAPS (c) and Auger emission in the case of AEAPS (e) and the other one describing processes with the excited $4f$ level being actively involved in the decay processes [(d), (f)]. The occupied parts of the band structure (shaded areas) and a second core level with energy E_c which is actively involved in the decay processes are included.

states is widely neglected.

According to the two-step model the main section of the paper (Sec. V) is organized as follows: In Sec. V A the excitation step is discussed. It will be shown that the combination of DAPS and CEELS data is well suited to obtain information about the different excitation processes in APS. In Sec. V B the influence of the different decay channels on the APS fine structure is discussed using SXAPS and AEAPS data. But first some experimental details (Sec. III) and aspects of data processing (Sec. IV) are presented.

III. EXPERIMENTAL

A. Apparatus

The experiments have been carried out in an ultrahigh-vacuum system with a pressure of about 1×10^{-10} mbar during the measurements. All measurements have been performed within the same recipient equipped with an x-ray detector for SXAPS and a cylindrical mirror analyzer (CMA) for energy-selective electron detection.

The x-ray detector uses a specially designed CsI-coated photocathode and the photocurrent is amplified by a microchannelplate. Different metal foils mounted on a rotary feedthrough have been used as x-ray filters for SXAPS to suppress selectively certain parts of the x-ray emission spectrum.

The CMA was used for AEAPS, DAPS, and CEELS. The energy resolution was about 0.6%. The AEAPS spectrum of LaB_6 has been taken with the analyzer energy held fixed in the region of the $\text{La } M_{4,5}N_{4,5}N_{4,5}$ Auger features and the incident-electron energy has been

scanned. In DAPS the intensity of the elastically scattered electrons is measured as a function of the primary energy. The energy of the analyzer had to be scanned simultaneously with the energy of the incident primary electrons. The CEELS experiment has been performed in constant final state mode; in this case the analyzer energy has been held fixed with the incident-electron energy being varied.

A commercially available electron gun (LEG22, Vacuum Generators) has been equipped with an indirectly heated cathode and was used as electron source in all experiments.

All spectra have been taken in derivative mode with lock-in techniques. The modulation voltage has been applied to the sample in APS and to the cathode of the electron gun in CEELS.

B. Energy calibration

In order to establish a common energy scale for APS and CEELS it was necessary to perform a careful energy calibration concerning the primary electron energy for APS as well as the loss energy for CEELS.

In a first step the primary energy of the incident electrons has been determined with an isochromat of silver taken with well-known photon energy. The isochromat has been taken as edge isochromat²² at a photon energy $\hbar\omega_0 = 72.7$ eV (Ref. 23) using the Al $L_{2,3}$ edge of a 0.75- μm Al foil as absorption edge. The foil has been placed in front of the x-ray detector. This experiment can be performed in any SXAPS apparatus equipped with an appropriate absorption foil without the need of further equipment. It seems therefore to be a convenient method for an absolute energy calibration in APS and will be discussed in the following.

The primary energy of the incident electrons measured with respect to the Fermi energy of the sample is given by the accelerating voltage U between electron emitter and sample and a constant energy parameter ϕ_{eff} including the work function of the emitter and the mean thermal energy of the emitted electrons

$$E_P = eU + \phi_{\text{eff}}. \quad (1)$$

ϕ_{eff} can be determined from the isochromat of silver from the relation

$$\hbar\omega_0 = eU_F + \phi_{\text{eff}} \quad (2)$$

with eU_F denoting the energy position of the Fermi edge E_F in the isochromat and U_F the corresponding accelerating voltage.²⁴ In the case of silver E_F can be determined as the maximum in the derivative of the measured isochromat.²⁵ The edge isochromat of polycrystalline silver is shown in Fig. 2 as a function of the accelerating voltage U . From $U_F = 70.2 \pm 0.2$ V it follows $\phi_{\text{eff}} = 2.5 \pm 0.2$ eV. This value has been used for absolute energy calibration of the incident electrons in all APS spectra.

In a second step the analyzer energy has been calibrated for energy-loss spectroscopy. The loss energy E_L is the difference between the primary energy E_P and the

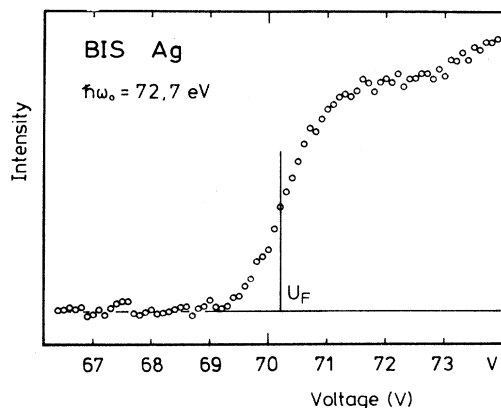


FIG. 2. Edge isochromat of silver taken at the $L_{2,3}$ edge of a 0.75- μm Al x-ray filter. The indicated accelerating voltage U_F corresponds to the position of the Fermi energy. The spectrum is used to calibrate the incident-electron energy for APS.

final-state energy E_f of the scattered electrons selected by the analyzer

$$E_L = E_P - E_f. \quad (3)$$

The determination of E_f has been performed by the detection of electrons scattered elastically at the surface of the sample with the incident electrons tuned to appropriate energy.

The energy-loss spectra should be taken at an energy as low as possible in order to facilitate a meaningful comparison with the APS spectra. The energy-loss spectra shown in this work have been taken at $E_f = 82$ eV. A further decrease in energy would require sampling times of several days since the signal-to-background ratio at lower energies is drastically reduced due to an enhanced background of secondary electrons.

C. Sample preparation

The polycrystalline hot-pressed hexaboride samples have been cleaned *in situ* by scraping with a diamond file. The CeO_2 sample has been prepared *in situ* as thin film by vacuum evaporation of Ce in an oxygen atmosphere of about 1×10^{-6} mbar during evaporation. It is known that CeO_2 is reduced to Ce_2O_3 during electron bombardment.²⁶ The spectra of CeO_2 have therefore been taken with low incident current density of about 0.1 mA/cm² and the sample was exposed to an oxygen atmosphere of 2×10^{-8} mbar during the measurements.²⁷ The cleanness of all samples was monitored by AES.

IV. DATA PROCESSING

The raw data have been taken in derivative mode with lock-in techniques. All spectra are affected by instrumental broadening resulting from the energy width of the incident electrons and the finite modulation amplitude. In the energy-loss spectra additional broadening occurs due to the finite resolution of the energy analyzer. The various broadening functions have been determined experimentally and all spectra except the isochromat of silver

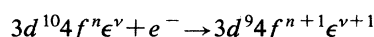
have been deconvoluted with the corresponding resolution functions by a Fourier transform formalism. Additionally, a linear background has been subtracted from the spectra.

Our spectra have been reintegrated numerically and are given in derivative form only if particular details of the fine structures are discussed. Accordingly, within this paper the expression "intensity of the spectrum" always means the intensities of the reintegrated spectra.

V. RESULTS AND DISCUSSION

A. The excitation step

From La and Ce x-ray emission and isochromat data²⁸⁻³⁰ it is known that the $3d \rightarrow 4f$ excitation by electron impact is resonantly enhanced near the excitation threshold due to formation of quasidecrete states of the $3d^9 4f^{n+2}$ configuration [Fig. 1(a)] with both the incident and the excited core electron captured by the $4f$ level (n denotes the number of localized $4f$ electrons in the ground state). It has been suggested that this excitation channel might be of importance also in the discussion of APS spectra.³¹⁻³³ The second excitation channel [Fig. 1(b)] which might contribute significantly to the APS signal leads to the $3d^9 4f^{n+1}$ configuration—known from our energy-loss spectra and from x-ray absorption spectroscopy³⁴⁻³⁸—with one electron being excited to the $4f$ level and the other one to a band state. There have been several suggestions concerning the relative contributions of both excitation channels



to the APS signal^{7,39-41} (ν denotes the number of itinerant electrons). From a comparison of La XAS and APS data Kanski *et al.*³³ concluded that the low-energy peak in their SAXPS spectrum reflects the La $3d^9 4f^1$ configuration whereas the main peak was attributed to the $3d^9 4f^2$ configuration. The interpretation of APS fine structure from a comparison with XAS data is, of course, somewhat problematic since in x-ray absorption only those transitions contribute to the signal which are not forbidden by dipole selection rules whereas in electron-excited spectra these restrictions are weakened.^{27,42-46} La for example shows a pronounced double-peak structure in the $3d$ energy-loss spectrum (Fig. 3) due to exchange splitting of the $3d^9 4f^1$ configuration; but in XAS the corresponding low-energy peak is completely suppressed.³⁴⁻³⁸

For a detailed understanding of the APS excitation step it is more informative to compare APS data with corresponding CEELS than with XAS data since both the APS and CEELS processes—especially at low energies—are not restricted by dipole selection rules. Of course, there exist some differences in the excitation processes between APS and CEELS leading to differences with respect to the spectral shapes when exciting the $3d^9 4f^{n+1}$ configuration. This will be discussed in the following.

Since the work of Kanski and Wendin⁴⁷ on CEELS of

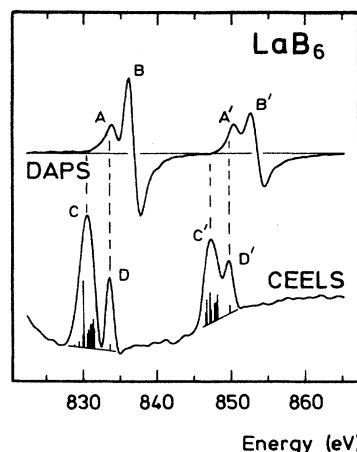


FIG. 3. DAPS and CEELS of the La $3d_{3/2,5/2}$ levels in LaB_6 . The spectra are presented on a common energy scale with DAPS given as a function of incident energy and CEELS as a function of loss energy. DAPS is given in derivative form and CEELS in nonderivative form. The La $3d^9 4f^1$ multiplet structure (bar diagram) has been taken from Thole *et al.* (Ref. 38). Dashed lines indicate the energy positions of the CEELS line structures.

light RE's it is known that the shapes of the double-peak structures of the $3d$ energy-loss spectra strongly depend on the final state energy E_f of the scattered electrons. According to Matthew *et al.*⁴⁴ this dependence is based on the variation of the cross-section ratio for dipole and nondipole excitations with varying incident energy. At rather high E_f in the order of or greater than the threshold energy, dipole-allowed transitions are favored and the CEELS double-peak structure is dominated by the high-energy peak. On the other hand, when E_f tends towards zero the cross section for nondipole transitions increases and the low-energy peak gains more and more intensity. The CEELS excitation $3d^{10} 4f^n \epsilon^\nu + e^- \rightarrow 3d^9 4f^{n+1} \epsilon^\nu + e^- [E_f]$ in the low-energy limit $E_f \rightarrow 0$ tends to the same electronic configuration as the corresponding APS excitation $3d^{10} 4f^n \epsilon^\nu + e^- \rightarrow 3d^9 4f^{n+1} \epsilon^{\nu+1}$ at the threshold. As in CEELS at low energies APS excitations of this type should therefore be dominated by nondipole transitions. To decide whether there is a significant contribution of this type of excitations to the APS signal the APS data should be compared with CEELS data taken at sufficiently low final energies E_f . We have chosen $E_f = 82$ eV which is less than 10% of the $3d$ threshold energy and low enough to reveal the complete multiplet structure of the $3d^9 4f^{n+1}$ configurations. The comparison of APS and CEELS data is further complicated by the fact that APS will not reflect the multiplet structure of the $3d^9 4f^{n+1}$ configuration directly because of the presence of the additional electron probing the density of the unoccupied extended states,⁴⁸ i.e., $D(E)[1-f(E)]$. $D(E)$ describes the one-particle density of states and the Fermi function $f(E)$ describes the occupation probability. Because of the localized character of the $4f$ level the total charge of the RE ion is not significantly altered upon the excitation $3d^{10} 4f^n \rightarrow 3d^9 4f^{n+1}$ and the density

of the extended states will not be affected very much by the excitation step. That part of the APS structure which is assumed to be associated with the $3d^9 4f^{n+1}$ configuration should then be given approximately by the convolution of the $3d^9 4f^{n+1}$ multiplet structure with the density of the unoccupied extended states $D(E)[1-f(E)]$ and with a Lorentzian describing the lifetime broadening. According to the ideas mentioned above the convolution production of the multiplet structure and the Lorentzian corresponds to our energy-loss spectrum. Thus, replacing the multiplet structure by the intensity $I_{\text{CEELS}}(E)$ of the energy-loss spectrum, one gets approximately

$$I_{\text{APS}}^{n+1}(E) \approx I_{\text{CEELS}}(E) * \{D(E)[1-f(E)]\} \quad (4)$$

where $I_{\text{APS}}^{n+1}(E)$ is confined to that part of the APS structure which is associated with the $3d^9 4f^{n+1}$ configuration. At room temperature the density of the unoccupied extended states in metals is characterized by a sharp rise at the Fermi energy so that near the excitation threshold $D(E)[1-f(E)]$ may be replaced by a step function. Then the convolution [Eq. (4)] simply yields the integral of I_{CEELS} . The derivative gives

$$I_{\text{CEELS}} = c \frac{d}{dE} (I_{\text{APS}}^{n+1}) \quad (5)$$

where I_{CEELS} is given as a function of loss energy and I_{APS}^{n+1} as a function of incident electron energy. For the $3d^9 4f^{n+1}$ spectral features Eq. (5) gives a simple relation between CEELS and APS concerning the shapes as well as the energy positions.

If there were any $3d^9 4f^{n+1}$ features present in the APS spectrum they should coincide with the CEELS features if the APS spectrum is given in derivative form and the CEELS spectrum in nonderivative form. This comparison is performed in Fig. 3 for the La $3d_{5/2}$ and $3d_{3/2}$ levels of LaB₆. We have chosen DAPS as the adequate APS version since DAPS is assumed to probe the APS excitation step in the most direct way. The La $3d^9 4f^1$ multiplet structure included in Fig. 3 has been calculated in intermediate coupling by Thole *et al.*³⁸ For each spin-orbit level the CEELS spectrum shows a main line (C, C') and a smaller narrow line on the high-energy side (D, D'). The narrow lines are caused by dipole-allowed transitions corresponding to nominal 3D_1 and 1P_1 multiplet terms which are the only terms containing considerable 1P_1 admixture.^{34,49} These lines correspond with the dominating lines in the x-ray absorption spectrum. The two main lines of the energy-loss spectrum are due to dipole-forbidden transitions corresponding to sets of 11 and 7 multiplet terms for the $3d_{5/2}$ and $3d_{3/2}$ levels, respectively. The derivative of the DAPS spectrum shows a main line (B, B') with a pronounced undershoot and a leading peak (A, A') on the low-energy side. In accordance with the La XAS result of Kanski *et al.*³³ the leading peaks A, A' of the APS spectrum coincide in energy with the $3d^{10} 4f^0 \rightarrow 3d^9 4f^1$ dipole-allowed transitions of the CEELS spectrum. But as the most important fact the CEELS main lines (C, C') clearly have no counterparts in DAPS. Thus, as a result, the DAPS spectrum

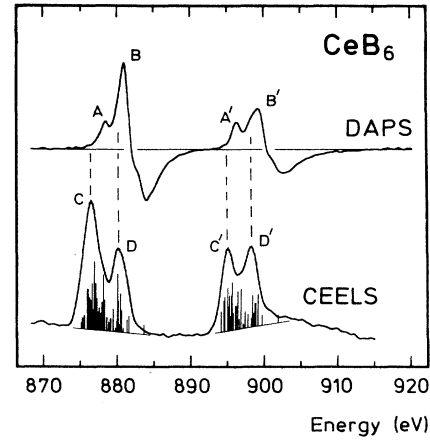


FIG. 4. DAPS and CEELS of the Ce $3d_{3/2,5/2}$ levels in CeB₆. The spectra are presented on a common energy scale with DAPS given as a function of incident energy and CEELS as a function of loss energy. DAPS is given in derivative form and CEELS in nonderivative form. The Ce $3d^9 4f^2$ multiplet structure (bar diagram) has been taken from Thole *et al.* (Ref. 38). Dashed lines indicate the energy positions of the CEELS line structures.

exhibits no $3d^9 4f^1$ features that may be associated with nondipole excitations. According to the ideas mentioned above these features should be present if there were any $3d^9 4f^1$ contribution at all. We therefore conclude that it is not the La $3d^9 4f^1$ configuration which causes the low-energy APS peaks, A, A' but the $3d^9 4f^2$ configuration.

In Fig. 4 analogous results are presented for Ce in CeB₆. The spectra again show a double-peak structure but exhibit a more complex fine structure due to the presence of the additional $4f$ electron in the ground state. And again the correspondence between APS and CEELS features is rather poor. In particular the low-energy peaks of the two spectra do not coincide in energy but are located at markedly higher energies in APS as compared with CEELS.

Taking both the La and Ce results together it seems to be very unlikely that there is a significant admixture of the $3d^9 4f^{n+1}$ configuration in the APS spectra. We therefore assume that the $3d^9 4f^{n+2}$ configuration is responsible not only for the APS main peaks but also for the low-energy peaks. The double-peak structure of the APS spectra—in nonderivative form—is then given by the multiplet splitting of the $3d^9 4f^{n+2}$ configuration broadened by lifetime effects.

For further insight into the APS excitation process the multiplet structure of the $3d^9 4f^{n+2}$ configuration is needed. Since no calculated data are available for La or trivalent Ce the discussion is extended in the following to tetravalent Ce. It is known that the APS spectrum of nominally tetravalent Ce in CeO₂ reflects excitations $3d^{10} 4f^0 + e^- \rightarrow 3d^9 4f^2$.²⁰ An additional DAPS measurement has therefore been performed on CeO₂. The spectrum is given in Fig. 5 in nonderivative form together with the corresponding $3d^9 4f^2$ multiplet structure given as a CEELS result from trivalent Ce in CeB₆ and as a calculated bar diagram from Thole *et al.*,³⁸ both taken from

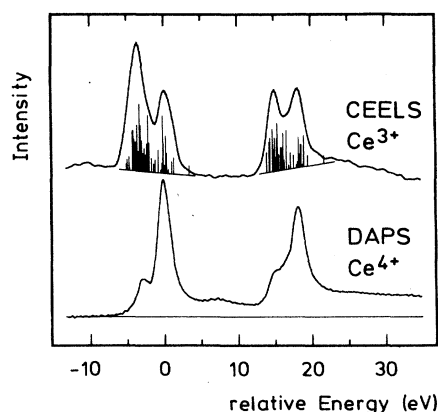
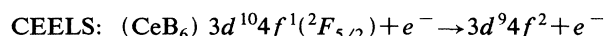
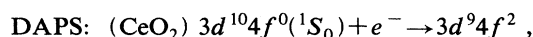


FIG. 5. Comparison of the Ce $3d^9 4f^2$ fine structure as seen with CEELS of trivalent cerium in CeB_6 and DAPS of tetravalent cerium on CeO_2 . The spectra have been adjusted to the maxima of the $3d_{5/2}$ structures. The result of an intermediate coupling calculation of the Ce $3d^9 4f^2$ multiplet structure from Thole *et al.* (Ref. 38) has been included as a bar diagram.

Fig. 4.

According to the two-step model the fine structure of the spectra should reflect the excitations



with different ground states and different transition processes but in this special case both leading to the same excited configuration $3d^9 4f^2$. So, if the fine structure of the DAPS spectrum was determined solely by the multiplet structure of the excited configuration one would expect similar fine structures in DAPS and CEELS. But the experimental results in Fig. 5 display a drastically different behavior: while the double-peak structure of the CEELS data agrees quite well with the calculated multiplet structure the DAPS spectrum is dominated by the high-energy part of the multiplet structure and the low-energy part is drastically reduced. We conclude from these data that the excitation cross sections in APS are strongly term dependent. From CEELS it is known that state-selective excitation probabilities play an important role in electron impact excitation near the threshold⁴⁴⁻⁴⁶ and APS is of course extremely a near-threshold technique. The different behavior of CEELS and APS data in Fig. 5 must then be attributed to the different excitation processes. We conclude therefore that the excitation probabilities of the two peaks differ significantly in APS and CEELS. In CEELS it is the increase of spin-flip processes and other nondipole transitions near the excitation threshold that reveals the complete multiplet structure of the excited configuration. In APS the situation is drastically different: there is no outgoing electron present in the excited state and therefore spin-flip processes are impossible. As a consequence, in the special case of the singlet ground state (1S_0) of Ce^{4+} in CeO_2 only those multiplet terms containing considerable doublet admixture will contribute significantly to the APS signal and quartet states will be effectively suppressed.

In conclusion the APS spectra of La and Ce compounds are caused by excitations $3d^{10}4f^n + e^- \rightarrow 3d^9 4f^{n+2}$. The fine structure is given by the multiplet structure of the excited configuration modified by state-selective excitation probabilities. For a more detailed analysis multiplet calculations including excitation probabilities have to be performed for the APS excitation process.

It is the scope of the following chapter to demonstrate that—in the case of SXAPS—the fine structure is not determined by the excitation step alone but is further influenced by the APS decay step.

B. The decay step

DAPS, SXAPS, and AEAPS spectra agree in the gross features but show slightly different fine structures. This is demonstrated for LaB_6 in Fig. 6. The spectra are given in derivative form allowing one to compare the relevant spectral features in more detail. Normally, in SXAPS the total x-ray yield is detected as a function of incident energy. Our SXAPS spectrum has been taken with a $0.75\text{-}\mu\text{m}$ Al foil as x-ray filter to suppress the low-energy photons that do not contribute significantly to the SXAPS signal but reduce the signal-to-noise ratio. The resulting shape of the spectral features is identical with that one obtained without filter (not shown here). In accordance with the DAPS result also SXAPS and AEAPS show a double-peak structure for each spin-orbit level with main peaks B, B' and leading peaks A, A' on the low-energy side. The most significant difference between DAPS and SXAPS concerns the intensity ratio B/A , respectively B'/A' , of the main peak and the leading peak. This ratio is several times larger in SXAPS than in DAPS for both

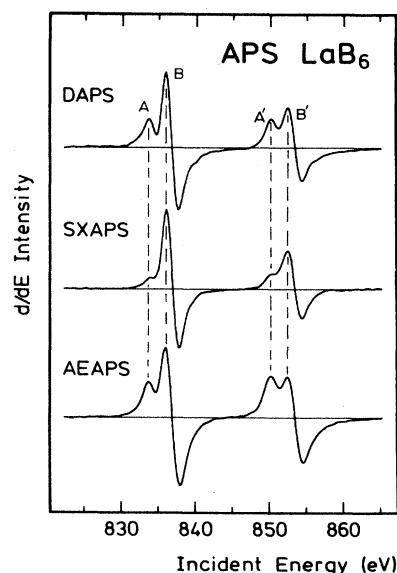
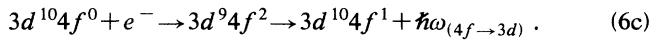
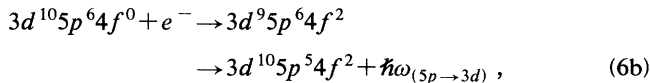
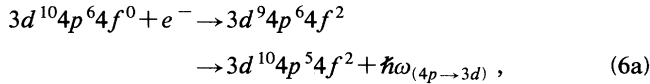


FIG. 6. APS spectra of lanthanum in LaB_6 given in derivative form. Dashed lines indicate the energy positions of the low-energy peaks A, A' and the main lines B, B' . The different APS versions show different peak-height ratios A/B and A'/B' .

spin-orbit levels. On the other hand DAPS and AEAPS give quite similar spectra. Since, in terms of the two-step model, the excitation step is the same for all APS spectra it seems to be the decay step of SXAPS that is responsible for the differences in the fine structures of SXAPS and DAPS or AEAPS. We have therefore performed an analysis of the different x-ray emission channels that contribute to the SXAPS intensity. In the special case of a $4f^0$ ground state there are mainly three channels available for the SXAPS process:



The decay steps of the channels (6a) and (6b) describe characteristic x-ray emission with the $3d$ hole converted into a $4p$ or $5p$ hole. The decay step of channel (6c) describes the x-ray recombination process where the $3d$ hole is filled up with one of the excited $4f$ electrons. This channel has been interpreted in x-ray emission spectroscopies as a resonant bremsstrahlung process.^{28,29}

The total SXAPS intensity is given as the sum of the emission of these three decay channels

$$I_{\text{SXAPS}} = I_{(4p \rightarrow 3d)} + I_{(5p \rightarrow 3d)} + I_{(4f \rightarrow 3d)}. \quad (7)$$

It has been suggested that the x-ray recombination channel (6c) might produce the dominating part of the SXAPS intensity.^{31,50,51} To clarify this point a detailed analysis of the SXAPS decay step has been performed with different metal foils as x-ray filters—a $0.75\text{-}\mu\text{m}$ Al foil and a $0.75\text{-}\mu\text{m}$ Fe foil—which discriminate between the different decay channels. Figure 7 illustrates the effect of the different filters. The transmission of the filters is given as a function of the photon energy and the bars indicate the energy positions of the La and Ce x-ray lines. The main function of the Al filter is to suppress the low-energy photons thus improving the signal-to-noise ratio, and both the characteristic x rays and the recombination x rays are detected. On the other hand the Fe foil completely suppresses the emission of the x-ray recombination channel and only the $4p \rightarrow 3d$ characteristic emission is detected. The comparison of the differently filtered SXAPS signals should then reveal information about the relative contributions of the different decay channels.

Figure 8 shows the SXAPS results for LaB_6 in derivative form. The spectrum filtered with the Fe foil has been smoothed and its intensity has been expanded by a factor of 45. The following discussion is performed for the $3d_{5/2}$ level but the conclusions are also valid for the $3d_{3/2}$ level. The comparison reveals two main results: (i) The intensity of the SXAPS signal filtered with Al foil is about 45 times larger than the signal of the spectrum filtered with Fe foil and (ii) the intensity ratio A/B (low-energy peak/main peak) is different for the differently filtered SXAPS spectra but seems to be nearly the same in

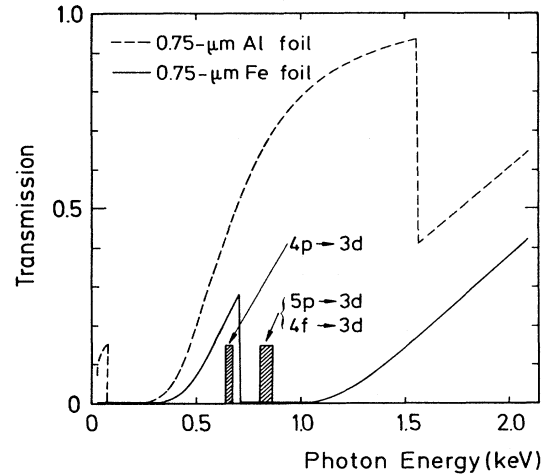


FIG. 7. Photon transmission factors for the different metal foils used in the SXAPS experiments (Ref. 52). The shaded areas indicate the energy positions of those La and Ce x-ray lines that contribute to the SXAPS signal.

SXAPS taken with the Fe foil and the AEAPS and DAPS spectra of Fig. 6.

Combining Eq. (7) with our first result (i) the relative contributions of the different decay channels (6a)–(6c) to the SXAPS intensity can be estimated. The measured SXAPS intensities have been corrected for the different transmission factors of the filters in the energy region of the corresponding x-ray emission lines. It follows that the $4p \rightarrow 3d$ emission channel produces only about 5–6% of the total SXAPS signal. Assuming now similar intensities for the characteristic emission channels $4p \rightarrow 3d$

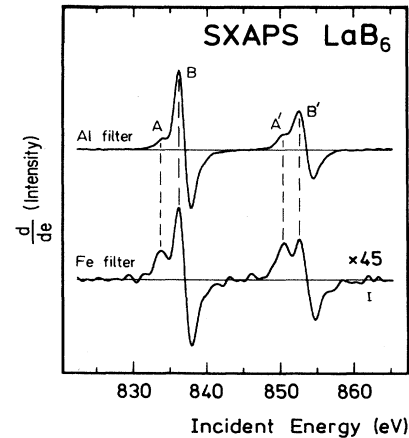


FIG. 8. SXAPS of lanthanum in LaB_6 taken with different metal foils as x-ray filters. The spectra are given in derivative form. Dashed lines indicate the energy positions of the low-energy peaks A , A' and the main lines B , B' . The iron foil suppresses completely the detection of photons resulting from the x-ray recombination process $3d^94f^2 \rightarrow 3d^{10}4f^1 + \hbar\omega$ leading to enhanced peak-height ratios A/B and A'/B' . The spectrum taken with the iron foil has been smoothed within the deconvolution procedure. The estimated statistical error is indicated by the error bar.

and $5p \rightarrow 3d$ which is expected from near-threshold x-ray emission data⁵³ the x-ray recombination emission $4f \rightarrow 3d$ contributes about 90% of the total SXAPS intensity.

This result is valid only for the intensity of the main SXAPS peak *B*. In the region of the low-energy peak *A* the change in intensity between the differently filtered spectra is much less dramatic. A quantitative analysis brings about roughly the same intensities for the x-ray recombination emission and the characteristic x-ray emission in this energy region. Thus the different peak-height ratio *A/B* in conventional SXAPS as compared with AEAPS and DAPS seems to be directly related to the $4f \rightarrow 3d$ emission of the x-ray recombination channel.

Similar conclusions can be drawn from the analogous CeB_6 data presented in Fig. 9. The intensity ratio of the two spectra is about 19; it follows that the x-ray recombination emission contributes about 72% of the intensity in the energy region of the main peak. This is not quite as high as for La but, nevertheless, it is high enough to cause obvious differences in the peak-height ratios *A/B* of the APS spectra.

From these results we conclude that the fine structure of the different APS spectra depends on the different character of the participating decay channels: if only characteristic emission contributes to the spectrum—Auger emission or characteristic x-ray emission—the set of excited multiplet terms as seen in DAPS is completely visible also in SXAPS and AEAPS. If, on the other hand, in conventional SXAPS the signal intensity is dominated by x-ray recombination emission the decay step serves as a “filter” suppressing certain parts of the excited multiplet structure. In the following an attempt will be made to explain this behavior as a consequence of dipole selection rules which apply to the x-ray emission step.

In the case of characteristic emission [(6a), (6b)] the SXAPS decay step consists of the radiative conversion of a $3d$ hole into a $4p$ or $5p$ hole. The final state configuration $3d^{10}p^54f^2$ offers a variety of multiplet terms and each one of the excited $3d^9p^64f^2$ multiplet states can decay via dipole transitions to $3d^{10}p^54f^2$ final states. Consequently the SXAPS spectrum contains all the features of the DAPS spectrum. Since the Auger emission process is not restricted by dipole selection rules all the DAPS features are also visible in AEAPS.

The situation is drastically different in conventional SXAPS where according to our conclusions the x-ray recombination channel is the dominating decay channel. In the special case of a $4f^0$ ground state the x-ray recombination process

$$3d^94f^2 \rightarrow 3d^{10}4f^1(^2F_{5/2,7/2}) + \hbar\omega_{(4f \rightarrow 3d)} \quad (8)$$

leads to the $4f^1$ final configuration with only two final states $^2F_{5/2}$ and $^2F_{7/2}$ available for the system in the decay step. As a consequence the number of the $3d^94f^2$ multiplet states that decay via the x-ray recombination channel is restricted by dipole selection rules to those terms that contain considerable 2D , 2F , or 2G admixture. The other terms will decay mainly via Auger transitions and—with rather low transition probabilities—via

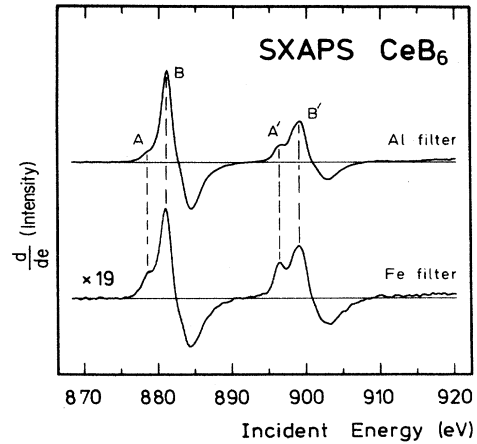


FIG. 9. SXAPS of cerium in CeB_6 taken with different metal foils as x-ray filters. The spectra are given in derivative form. Dashed lines indicate the energy positions of the low-energy peaks *A*, *A'* and the main lines *B*, *B'*. The iron foil suppresses completely the detection of photons resulting from the x-ray recombination process $3d^94f^3 \rightarrow 3d^{10}4f^2 + \hbar\omega$ leading to enhanced peak-height ratios *A/B* and *A'/B'*.

characteristic x-ray emission. They do not contribute significantly to the SXAPS intensity. The fine structure in (conventional) SXAPS should therefore mainly be given by the selected part of the $3d^94f^2$ multiplet structure that contains 2D , 2F , or 2G admixture.

In the special case of CeO_2 these conclusions can be tested independently by a comparison of SXAPS spectra with suitably chosen x-ray absorption data. With some restrictions the x-ray recombination process for a $4f^0$ ground-state system is equivalent to the inverse of an x-ray absorption process of the kind

$$3d^{10}4f^1(^2F_{5/2}) + \hbar\omega_{(4f \rightarrow 3d)} \rightarrow 3d^94f^2(^2D, ^2F, ^2G), \quad (9a)$$

$$3d^{10}4f^1(^2F_{7/2}) + \hbar\omega_{(4f \rightarrow 3d)} \rightarrow 3d^94f^2(^2D, ^2F, ^2G). \quad (9b)$$

The first transition (9a) equals an ordinary x-ray absorption process of trivalent cerium starting from the $j = \frac{5}{2}$ ground state. Transition (9b) describes an absorption process starting from the $j = \frac{7}{2}$ state which is separated from the ground state by the spin-orbit energy of about 0.3 eV. Both x-ray absorption spectra have been calculated in intermediate coupling by van der Laan *et al.*⁵⁴ We use a combination of both to perform a model calculation of the CeO_2 SXAPS spectrum. To account for the characteristic emission channel the intensity of our model spectrum includes a certain amount of the DAPS intensity leading to

$$I_{\text{model}} = c_1 I(^2F_{5/2}) + c_2 I(^2F_{7/2}) + c_3 I_{\text{DAPS}}. \quad (10)$$

$I(^2F_{5/2})$ and $I(^2F_{7/2})$ represent the intensities of the x-ray recombination channel with final states $4f^1(^2F_{5/2})$ and $4f^1(^2F_{7/2})$ as calculated by van der Laan *et al.*⁵⁴ for the absorption process [9(a) and 9(b)] and convoluted with a Lorentzian of 1.0 eV (full width at half maximum) to account for lifetime broadening. The intensity ratio of

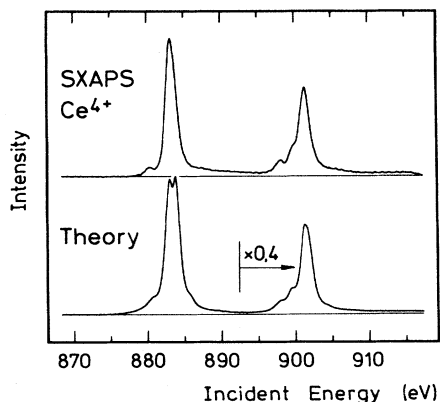


FIG. 10. Comparison of the experimental CeO_2 SXAPS spectrum and a model spectrum based on calculated XAS data (Ref. 54) and the experimental DAPS spectrum; for explanation see text. The calculated $3d_{3/2}$ structure has been reduced in intensity by a factor of 0.4.

the transitions involving the ${}^2F_{5/2}$ and ${}^2F_{7/2}$ states is assumed to be roughly the same for the emission process in SXAPS and the absorption process in XAS. Accordingly we have chosen $c_1 = c_2 = 1$. c_3 is taken from a fit of I_{model} to the experimental SXAPS spectrum so that $c_3 I_{\text{DAPS}}$ contributes about 15% to I_{model} .

In Fig. 10 the resulting model spectrum is compared with our CeO_2 SXAPS result. A good overall agreement between the fine structures of the two spectra is revealed except for some minor details. The model spectrum of the $3d_{3/2}$ level had to be reduced in intensity by a factor of 0.4 to agree with the experimental result. Similarly, anomalous intensities for the $3d_{3/2}$ structure have also been observed in resonant x-ray emission measurements on Eu (Ref. 55) and TbCo_2 (Ref. 56) and were attributed by Cramm *et al.*⁵⁵ to the conversion of the $3d_{3/2}$ hole into a $3d_{5/2}$ hole in the course of the direct recombination process $3d_{3/2}^9 4f^{n+1} \rightarrow 3d_{5/2}^9 4f^n + e^-$. A similar recombination process $3d_{3/2}^9 4f^{n+2} \rightarrow 3d_{5/2}^9 4f^{n+1} + e^-$ seems to act also in SXAPS of Ce leading to reduced SXAPS intensity for the $3d_{3/2}$ level.

As a further important result, the suppression of the low-energy APS features in SXAPS (Fig. 10) as compared with DAPS (Fig. 5) is described correctly by the model confirming the importance of the x-ray recombination channel in the decay step of SXAPS. This result does not depend on the proper choice of the parameters c_i .

On the other hand the fine structure as predicted by the model does not agree in full detail with the experimental result. While the fine structure of the $3d_{3/2}$ level is in excellent agreement with the experimental result the splitting of the $3d_{5/2}$ main peak into two linelike features as predicted by the model is not resolved in the experimental result. One should keep in mind that according to Eq. (10) our simple SXAPS model does not include the excitation step. State-dependent excitation probabilities are completely neglected. Differences in the fine structures between the model spectrum and the experimental SXAPS result seem to indicate that the excitation step is important not only for DAPS and AEAPS but also for

the SXAPS fine structure.

In conclusion the overall agreement between the model spectrum and the experimental SXAPS result is quite good supporting the basic ideas of our APS model. For a more detailed understanding of the APS fine structure state-dependent excitation cross sections have to be included in the model.

VI. SUMMARY AND OUTLOOK

A two-step model for the $3d$ APS process of light rare-earth compounds is worked out. The common features as well as the specific differences in SXAPS, DAPS, and AEAPS are discussed comprehensively. The close connection between APS and near-threshold CEELS spectra has been utilized to identify the important APS transition channels. The two-step description is based on APS data and near-threshold CEELS data taken from La and both trivalent and tetravalent Ce compounds yielding detailed information about the excitation and emission processes in APS. The $4f$ levels of the rare-earth compounds have been treated as discrete levels.

The APS excitation was found to be dominated by the resonant transition $3d^{10} 4f^n \epsilon^{\nu} + e^- \rightarrow 3d^9 4f^{n+2} \epsilon^{\nu}$ with both the incident electron and the $3d$ core electron being excited to the $4f$ level. Excitations $3d^{10} 4f^n \epsilon^{\nu} + e^- \rightarrow 3d^9 4f^{n+1} \epsilon^{\nu+1}$ with only one electron being excited to the $4f$ level and the other one to a band state seem to have no significant influence on the APS spectral features. The excited $3d^9 4f^{n+2}$ configuration predominantly decays via Auger transitions and—in the case of the $3d_{3/2}$ core hole—via the direct recombination process $3d_{3/2}^9 4f^{n+2} \rightarrow 3d_{5/2}^9 4f^{n+1} + e^-$ where the $3d_{3/2}$ hole is converted into a $3d_{5/2}$ hole. From the competing x-ray emission processes the recombination process $3d^9 4f^{n+2} \rightarrow 3d^{10} 4f^{n+1} + \hbar\omega$ is by far the dominating decay process.

The APS fine structure is given by the multiplet structure of the excited configuration $3d^9 4f^{n+2}$. But only a selected part of the $3d^9 4f^{n+2}$ multiplet terms contributes to the APS spectra; the major part is suppressed due to state-selective excitation probabilities which play an important role in APS near the excitation threshold. In the case of SXAPS the fine structure may be further influenced by the decay step due to dipole selection rules. This is particularly the case for $4f^0$ ground-state systems such as La compounds and CeO_2 : only those terms of the excited $3d^9 4f^2$ multiplet structure decay via the x-ray recombination channel that contain considerable 2D , 2F , or 2G admixture; other terms decay preferentially via nonradiative transition. As a consequence differences are observed in the fine structures of SXAPS and DAPS or AEAPS.

The SXAPS intensity of the $3d_{3/2}$ core level is reduced due to the occurrence of the direct recombination channel $3d_{3/2}^9 4f^2 \rightarrow 3d_{5/2}^9 4f^1 + e^-$ which converts the $3d_{3/2}$ hole into a $3d_{5/2}$ hole. These mechanisms explain well the observed differences in the fine structure of the APS spectra.

As the most important result, APS has turned out to be an appropriate tool for the investigation of the elec-

tronic structure of rare-earth compounds. The APS structure is related to the ground state of the RE system via the excitation $3d^{10}4f^{n+e^-} \rightarrow 3d^9 4f^{n+2}$. APS should, thus, be appropriate to determine ground-state properties in a way similar to other core-level spectroscopies such as XPS, XAS, and CEELS with the advantage of a rather simple experimental setup. In terms of atomiclike $4f$ states this has already been done successfully for γ -Ce and the oxides.¹⁹ An expansion beyond the atomiclike description including hybridization effects

and nonintegral $4f$ electron counts seems now to be possible.

ACKNOWLEDGMENTS

We would like to thank C. Sohn, J. Schnieder, U. Rolke, and C. Westphal for their valuable contributions in the course of this work. The financial support from the Deutsche Forschungsgemeinschaft (Bonn, Germany) is gratefully acknowledged.

*Present address: Fachbereich 02, Fachhochschule Münster, D-4430 Steinfurt, Federal Republic of Germany.

¹R. L. Park and J. E. Houston, *J. Vac. Sci. Technol.* **11**, 1 (1974).

²R. L. Park, *Surf. Sci.* **48**, 80 (1975).

³G. Ertl and J. Küppers, *Low Energy Electrons and Surface Chemistry* (VCH Verlagsgesellschaft mbH, Weinheim, 1985).

⁴J. Kirschner and P. Staib, *Appl. Phys.* **6**, 99 (1975).

⁵R. L. Gerlach, *Surf. Sci.* **28**, 648 (1971).

⁶J. E. Houston and R. L. Park, *Phys. Rev. B* **5**, 3808 (1972).

⁷J. Kanski and P. O. Nilsson, *Phys. Rev. Lett.* **43**, 1185 (1979).

⁸J. E. Houston, R. L. Park, and G. E. Laramore, *Phys. Rev. Lett.* **30**, 846 (1973).

⁹R. L. Park and J. E. Houston, *Phys. Rev. A* **7**, 1447 (1973).

¹⁰C. Webb and P. M. Williams, *Phys. Rev. Lett.* **33**, 824 (1974).

¹¹Y. Fukuda, W. T. Elam, and R. L. Park, *Phys. Rev. B* **16**, 3322 (1977).

¹²R. L. Park and J. E. Houston, *Phys. Rev. B* **6**, 1073 (1972).

¹³V. Dose and H. Scheidt, *Appl. Phys.* **19**, 19 (1979).

¹⁴S. W. Schulz, K.-Th. Schleicher, D. M. Rück, and H.-U. Chun, *J. Vac. Sci. Technol. A* **2**, 822 (1984).

¹⁵J. C. Fuggle, *Physica B+C* **130B**, 56 (1984).

¹⁶K. Schönhammer and O. Gunnarsson, *J. Magn. Magn. Mater.* **63&64**, 481 (1987).

¹⁷J. W. Allen, S. J. Oh, O. Gunnarsson, K. Schönhammer, M. B. Maple, M. S. Torikachvili, and I. Lindau, *Adv. Phys.* **35**, 275 (1986).

¹⁸W.-D. Schneider, B. Delley, E. Wuilloud, J.-M. Imer, and Y. Baer, *Phys. Rev. B* **32**, 6819 (1985).

¹⁹H. Hinkers, C. Westphal, and H. Merz, *J. Phys. (Paris) Colloq.* **48**, C9-1041 (1987).

²⁰H. Hinkers, R. Stiller, M. Merz, W. Drewes, and H.-G. Purwins, *Phys. Scr.* **36**, 166 (1987).

²¹J. C. Rivière, F. P. Netzer, G. Rosina, G. Strasser, and J. A. A. Matthew, *J. Electron Spectrosc. Relat. Phenom.* **36**, 331 (1985).

²²M. Conrad, V. Dose, Th. Fauster, and H. Scheidt, *Appl. Phys.* **20**, 37 (1979).

²³V. Dose, H.-J. Gossmann, and D. Straub, *Phys. Rev. Lett.* **47**, 608 (1981).

²⁴H. Merz, *Phys. Status Solidi A* **1**, 707 (1970).

²⁵J. K. Lang and Y. Baer, *Rev. Sci. Instrum.* **50**, 221 (1979).

²⁶E. Wuilloud, B. Delley, W.-D. Schneider, and Y. Baer, *Phys. Rev. Lett.* **53**, 202 (1984).

²⁷F. P. Netzer, G. Strasser, and J. A. D. Matthew, *Phys. Rev. Lett.* **51**, 211 (1983).

²⁸F. Riehle, Ph.D. thesis, Universität Karlsruhe, 1977.

²⁹R. J. Liefeld, A. F. Burr, and M. B. Chamberlain, *Phys. Rev. A* **9**, 316 (1974).

³⁰M. B. Chamberlain, A. F. Burr, and R. J. Liefeld, *Phys. Rev. A* **9**, 663 (1974).

³¹M. B. Chamberlain and W. L. Baum, *J. Vac. Sci. Technol.* **12**, 1047 (1975).

³²W. E. Harte, P. S. Szczepanek, and A. J. Leyendecker, *J. Less-Common. Met.* **93**, 189 (1983).

³³J. Kanski, P. O. Nilsson, and I. Curelaru, *J. Phys. F* **6**, 1073 (1976).

³⁴C. Bonnelle, R. C. Karnatak, and J. Sugar, *Phys. Rev. A* **9**, 1920 (1974).

³⁵J. M. Esteva, R. C. Karnatak, and J. P. Connerade, *J. Electron Spectrosc. Relat. Phenom.* **31**, 1 (1983).

³⁶P. Motais, E. Belin, and C. Bonnelle, *Phys. Rev. B* **30**, 4399 (1984).

³⁷G. Kaindl, G. Kalkowski, W. D. Brewer, B. Perscheid, and F. Holtzberg, *J. Appl. Phys.* **55**, 1910 (1984).

³⁸B. T. Thole, G. van der Laan, J. C. Fuggle, G. A. Sawatzky, R. C. Karnatak, and J. M. Esteva, *Phys. Rev. B* **32**, 5107 (1985).

³⁹R. J. Smith, M. Piacentini, J. L. Wolf, and D. W. Lynch, *Phys. Rev. B* **14**, 3419 (1976).

⁴⁰W. E. Harte and P. S. Szczepanek, *Phys. Rev. Lett.* **42**, 1172 (1979).

⁴¹D. Chopra, G. Martin, H. Naraghi, and L. Martinez, *J. Vac. Sci. Technol.* **18**, 44 (1981).

⁴²M. Inokuti, *Rev. Mod. Phys.* **43**, 297 (1971).

⁴³R. Ludeke and A. Koma, *Phys. Rev. Lett.* **34**, 817 (1975).

⁴⁴J. A. D. Matthew, G. Strasser, and F. Netzer, *Phys. Rev. B* **27**, 5839 (1983).

⁴⁵K. Nuroh, *J. Phys. C* **20**, 5305 (1987).

⁴⁶H. R. Moser and G. Wendin, *Solid State Commun.* **65**, 107 (1988).

⁴⁷J. Kanski and G. Wendin, *Phys. Rev. B* **24**, 4977 (1981).

⁴⁸G. Wendin, in *Vacuum Ultraviolet Radiation Physics*, edited by E. E. Koch, R. Haensel, and C. Kunz (Pergamon-Vieweg, Braunschweig, 1974), p. 252.

⁴⁹H. R. Moser, B. Delley, W.-D. Schneider, and Y. Baer, *Phys. Rev. B* **29**, 2947 (1984).

⁵⁰G. Wendin and K. Nuroh, *Phys. Rev. Lett.* **39**, 48 (1977).

⁵¹W. E. Harte, P. S. Szczepanek and A. J. Leyendecker, *Phys. Rev. Lett.* **33**, 86 (1974).

⁵²B. L. Henke, P. Lee, T. J. Tanaka, R. L. Shimabukuro, and B. K. Fujikawa, *At. Data Nucl. Data Tables* **27**, 1 (1982).

⁵³M. B. Chamberlain, A. F. Burr, and R. J. Liefeld, *J. Vac. Sci. Technol. A* **2**, 973 (1984).

⁵⁴G. van der Laan, B. T. Thole, G. A. Sawatzky, J. C. Fuggle, R. Karnatak, J. M. Esteva, and B. Lengeler, *J. Phys. C* **19**, 817 (1986).

⁵⁵S. Cramm, U. Grabowski, C. Kunz, J. Schmidt-May, F. Senf, and L. Inocchia, *J. Electron Spectrosc. Relat. Phenom.* **42**, 89 (1987).

⁵⁶J. W. Allen, S. J. Oh, I. Lindau, and L. I. Johansson, *Phys. Rev. B* **29**, 5927 (1984).